IOP Publishing and International Atomic Energy Agency Nuclear Fusion

Nucl. Fusion **48** (2008) 024016 (13pp) doi:10.1088/0029-5515/48/2/024016

Characterization of local turbulence in magnetic confinement devices

Milan Rajković[1], Miloš Škorić[2], Knut Sølna[3] and Ghassan Antar[4]

[1] Institute of Nuclear Sciences Vinča, Belgrade, Serbia
[2] National Institute for Fusion Science, 322-6 Oroshi-cho, Toki 509-5292, Gifu, Japan
[3] Department of Mathematics, University of California Irvine, CA 92697-3875, USA
[4] Department of Physics, American University of Beirut, PO Box 11-0236, Riad EL-Solh/Beirut 1107 2020, Lebanon

E-mail: milanr@vin.bg.ac.yu

Received 4 June 2007, accepted for publication 2 October 2007
Published 30 January 2008
Online at stacks.iop.org/NF/48/024016

Abstract

A multifractal analysis based on evaluation and interpretation of large deviation spectra is applied to plasma edge turbulence data from different devices (MAST and Tore Supra). It is demonstrated that in spite of some universal features there are unique characteristics for each device as well as for different confinement regimes. In the second part of the exposition the issue of estimating the variable power law behavior of spectral densities is addressed. The analysis of this issue is performed using fractional Brownian motion (fBm) as the underlying stochastic model whose parameters are estimated locally in time by wavelet scale spectra. In this manner information about the inertial range as well as variability of the fBm parameters is obtained giving more information important for understanding edge turbulence and intermittency.

PACS numbers: 52.35.Ra, 05.65.+b, 47.11.St, 47.53+n, 52.55.Fa

1. Introduction

Plasma edge turbulence, known for a long time to be intermittent in the scrape-off layer (SOL) [1], is the focus of intense current research efforts aimed at understanding plasma confinement and dynamics of turbulent transport in magnetic fusion devices which represent important issues related to the control of confined plasma. Turbulence studies of the SOL have revealed that intermittency in this region is caused by large-scale coherent structures with high radial velocity designated as blobs (or avaloids). A natural route for understanding turbulence and intermittency in the edge region of confinement devices and related transport properties is to search for universal properties and differences between dynamics of different systems and regimes. The first studies performed in this direction have concentrated on the search for long-range dependence properties of plasma density fluctuations as well as on their eventual self-similar properties [2, 3] and a similar treatment has also been applied to floating potential fluctuations [3]. Self-similar processes were attractive models to describe scalings of plasma fluctuations due to the fact that they are well documented and mathematically well defined. In addition they are relatively simple and parsimonious and each of their properties are controlled by the one unique parameter, H, known as the Hurst parameter. It was soon realized that in spite of observed self-similarity for several confinement devices, over the mesoscale range of time scales, i.e. scales between 10 times the turbulence decorrelation time and plasma confinement time, different scaling laws exist in different time-scale ranges. Hence, it became clear that self-similar processes are not adequate to model the extremely complex plasma turbulence fluctuations. The existence of long-range correlations, noticed in several magnetic confinement devices, suggested that scaling models with a single parameter are appropriate at large temporal scales but at small scales, characteristic of intermittency, more parameters are needed. As a consequence, a need for multifractal analysis, an extension of monofractal analysis which is based on the self-similarity concept, was recognized recently. In spite of that, only a few studies were devoted to the multifractal analysis of plasma fluctuations and, more importantly, the multifractal analysis tools used were inadequate to recognize subtle differences in various confinement devices and hence deviations from universal characteristics [4–7].

Plasma turbulence studies usually rely on results obtained for neutral fluid turbulence which may be beneficial from many aspects although care must be taken in recognizing differences and specific features of each. In particular, nonlinearities in plasma turbulence are more numerous having different spectral cascade directions in addition to the $E \times B$ nonlinearity, leading to more complex fluctuating characteristics. One of the most important differences is that time and space measurements lead to different information on the structure of turbulence [6].

Driving mechanisms and damping characteristics are reflected in the temporal aspect of fluctuations while measurements at different spatial locations provide information on spatial structures for various scale lengths. For the case of neutral fluids, time records of turbulent velocity at a single spatial location obtained with the use of a hot-wire or laser Doppler anemometer are usually interpreted via Taylor's frozen flow hypotheses, as one-dimensional spatial cuts through the flow. However, this approach that generates information about temporal measurements from spatial ones and vice versa is not applicable in the case of plasma turbulence. Specifically, turbulence in the case of neutral fluids is generated at a certain spatial position and carried by the flow past the probe location so that recordings at different times at a fixed location are equivalent to simultaneous recordings at different spatial locations along the flow. However, in plasma turbulence due to the specific nature of nonlinearities, turbulence is created and damped at the same spatial position where measurements are taken so that spatial and temporal information is interwoven. For the same reason the inertial range [8] may exist only locally in space or in time, and the extent of this range changes along the temporal scale as well as along space, for example, along the poloidal direction. One of the main results of the study presented here is to establish the existence of local (in time) inertial range and to estimate its scaling properties for various devices and confinement regimes. Proving the existence of local inertial range and evaluating its characteristics may be of great importance, among other things, in generating synthetic random media for simulation of wave propagation in turbulent plasma, relevant for Doppler reflectometry, for example.

One of the first important issues to be agreed upon in the analysis of plasma turbulence, and in particular intermittency and its multifractal character, is the choice of relevant measure. In neutral fluid turbulence, in addition to velocity, enstrophy and energy dissipation represent quantities of particular interest although they cannot be constructed in their entirety from a single point velocity time-series. These quantities are usually replaced by the so-called surrogate fields which take the form of a single component of many component fields. Intermittency is usually studied via energy dissipation rate whose complete expression is given by

$$\epsilon(\vec{r}) = \frac{\nu}{2}\sum_{i,j}\left(\frac{\partial v_i}{\partial x_j} + \frac{\partial v_j}{\partial x_i}\right)^2, \tag{1}$$

where ν is kinematic viscosity (viscosity divided by the fluid density), v_i is the i component of velocity and x_i are spatial coordinates. This expression evidently cannot be constructed from recorded time-series as usually only the longitudinal and transverse components of velocity, v_x and v_y, respectively, are measured. To overcome the difficulty, expression (1) is replaced by the so-called surrogate dissipation

$$\epsilon_{\mathrm{surr}}(x) = C\nu\left(\frac{\partial v_x}{\partial x}\right)^2, \tag{2}$$

where C is a constant, sometimes taken equal to 15 [9]. Using Taylor's frozen flow hypothesis which is naturally justified in neutral fluid turbulence, expression (2) becomes

$$\epsilon_{\mathrm{surr}}(t) \sim \nu\left(\frac{\partial v_x}{\partial t}\right)^2. \tag{3}$$

An important measure quantifying intermittency is the so-called intermittency exponent. As proposed in [10], it may be extracted from the slope of the two-point correlation function of the energy dissipation field. This procedure may be used to develop a criterion for constructing a measure, analogous to the surrogate dissipation, relevant for plasma turbulence and intermittency. In [11], it was demonstrated that normalized two-point correlation function $\langle\epsilon_{\mathrm{surr}}(x+\Delta x)\epsilon_{\mathrm{surr}}(x)\rangle/\langle\epsilon_{\mathrm{surr}}(x)\rangle^2$ scales as $\sim \Delta x^{-\mu}$, where μ is the intermittency exponent. Studies in this reference and in [9] , for the case of atmospheric turbulence, and studies in [12] and [13], for the gaseous helium jet, found $\mu \simeq 0.22$, independent of the Reynolds number.

In the exposition that follows we assume that ion saturation current fluctuations, the only measured quantity used in this exposition, are equivalent to density fluctuations as justified in detail in [14] . Based on the above description for the case of neutral fluid turbulence, we set as the goal construction of a measure analogous to surrogate dissipation whose scaling of two-point correlation function of L-mode fluctuations would yield an intermittency exponent as close to the value for neutral fluid turbulence as possible. The reason for choosing L-mode fluctuations is supported by results presented further on in this study, which imply that L-mode intermittent fluctuations are very similar in their fractal and multifractal aspects to the neutral fluid intermittency. A search for an appropriate measure, based on heuristic arguments, was described in [6], and proposed measures are

$$\epsilon_n = \frac{(n-\langle n\rangle)^2}{\langle(n-\langle n\rangle)^2\rangle} \tag{4}$$

and

$$\epsilon_{\delta n} = \frac{\left(\dfrac{\mathrm{d}n}{\mathrm{d}t} - \left\langle\dfrac{\mathrm{d}n}{\mathrm{d}t}\right\rangle\right)^2}{\left\langle\left(\dfrac{\mathrm{d}n}{\mathrm{d}t} - \left\langle\dfrac{\mathrm{d}n}{\mathrm{d}t}\right\rangle\right)^2\right\rangle}. \tag{5}$$

A similar measure with $\mathrm{d}n^2/\mathrm{d}t$ replacing $\mathrm{d}n/\mathrm{d}t$ in (5) was employed in [14]. However our study based on the analysis of L-mode fluctuations in MAST, Tore Supra and PISCES devices indicates that these two measures yield too high or too low values for the intermittency exponent. The following two measures

$$\epsilon = c\cdot\frac{\left(\left|n\dfrac{\mathrm{d}n}{\mathrm{d}t}\right| - \left\langle\left|n\dfrac{\mathrm{d}n}{\mathrm{d}t}\right|\right\rangle\right)^2}{\left\langle\left(\left|n\dfrac{\mathrm{d}n}{\mathrm{d}t}\right| - \left\langle\left|n\dfrac{\mathrm{d}n}{\mathrm{d}t}\right|\right\rangle\right)^2\right\rangle} \tag{6}$$

and

$$\epsilon = c\cdot\frac{\left(\left(n\dfrac{\mathrm{d}n}{\mathrm{d}t}\right)^2 - \left\langle\left(n\dfrac{\mathrm{d}n}{\mathrm{d}t}\right)^2\right\rangle\right)^2}{\left\langle\left(\left(n\dfrac{\mathrm{d}n}{\mathrm{d}t}\right)^2 - \left\langle\left(n\dfrac{\mathrm{d}n}{\mathrm{d}t}\right)^2\right\rangle\right)^2\right\rangle}, \tag{7}$$

where c is a constant, which upon evaluation of the slope of two-point correlation function yield intermittency exponent $\mu \sim 0.3$, a value closer to the μ of neutral fluid intermittency

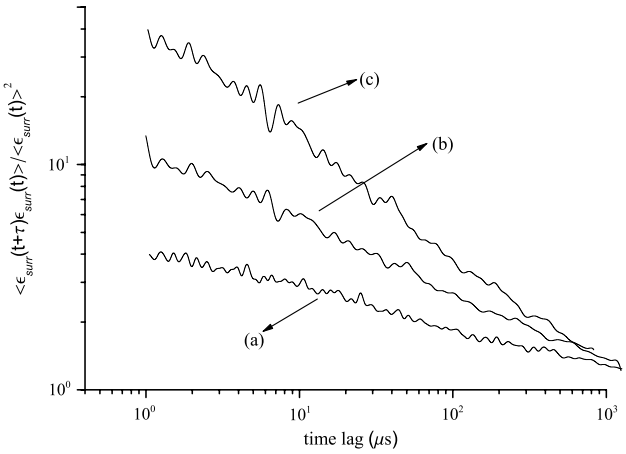

Figure 1. Normalized two-point correlation function of the surrogate dissipation measures obtained from the MAST 6861 L-mode density fluctuations. In the evaluation of two-point correlators the measures used were (a) equation (4) or equation (5), (b) equation (6) or equation (7) and (c) equation (5) with dn^2/dt replacing dn/dt. Measures were filtered with the Wiener filter and (b) yields the optimal slope value $\sim .0.3$.

than the values obtained from two-point correlation functions of measures (4) and (5). Following Wiener filtering[5] of surrogate dissipation measures given by expressions (4), (5) and (6) the obtained two-point correlators are compared in figure 1 for the case of L-mode MAST ion saturation fluctuations. Two-point correlation functions from measures (6) and (7) yield the same slope so only one is presented in the figure. The same slope values were obtained for the Tore Supra data. It should be emphasized that measures in expressions (6) and (7) are by no means expressions for dissipation but rather surrogate quantities whose multifractal and two-point correlation function properties give accurate information about the burstiness property of the ion saturation current (i.e. plasma density). Namely, one kind of burstiness arises from dependences over long time periods as reflected in the long-range correlation property and the second kind of burstiness arises from fluctuations in amplitude and therefore concerns small scale behaviour. These two types of burstiness are well captured and quantified within the multifractal formalism by measures that we propose here, (6) and (7).

The rest of the paper is organized as follows. In section 2 we present basic features of multifractal processes with special emphasis on large deviation spectra. In section 3 we present multifractal characteristics of L-mode and dithering H-mode of the MAST device and the L-mode of the Tore Supra device. This analysis is based on the large deviation spectra which reveal features unobtainable using the traditional Legendre or Hausdorff multifractal spectra. In section 4 local features of turbulence are modelled using fractional Brownian motion (fBm) and wavelet techniques, and results pertaining to the two devices of section 3 are considered. Finally, in section 5 we present our conclusions related to the universal and idiosyncratic aspects of results obtained.

[5] Wiener filtering mostly affects derivatives of the data so that the outcome is particularly apparent in logarithmic coordinates. Its importance in the context of neutral fluid turbulence may be found in [11].

2. Multifractal measures and properties

Multifractal measures can be built by iterating a simple procedure called a *multiplicative cascade* whose various forms are used to model the energy dissipation field of fully developed turbulence, physically motivated by the Richardson cascade model of energy transfer from large to small scales by random breakup of eddies. The simplest example of such cascades is the binomial measure on $I = [0, 1]$ (e.g. [15]). Consider the uniform probability measure μ_0 on I, and split the unit interval I into two subintervals $I_0 = [0, 1/2]$ and $I_1 = [1/2, 1]$. In the process mass m_0 is spread uniformly over I_0 and m_1 is spread over I_1 so that $m_1 = 1 - m_0$ and it is obvious that the density of measure μ_1 is a step function. With the two subintervals the procedure is repeated in the same manner so that at the second stage the measures are $\mu_2[I_{00}] = m_0m_0$, $\mu_2[I_{01}] = m_0m_1$, $\mu_2[I_{10}] = m_1m_0$ and $\mu_2[I_{11}] = m_1m_1$. At stage n, the conserved mass equal to 1 is distributed among the 2^n dyadic intervals $I_{\varepsilon_1\ldots\varepsilon_n}$ according to all possible products $\mu(I_{\varepsilon_1\ldots\varepsilon_n}) = m_{\varepsilon_1}\ldots m_{\varepsilon_n}$, where m_{ε_i} are denoted as multipliers. Iteration of this procedure generates an infinite sequence of measures $\{\mu_n\}$ that weakly converge to the binomial measure μ. The construction creates large and increasing heterogeneity in the allocation of mass leading to the multifractal properties. The binomial, like many multifractals, is a continuous but singular probability measure that has no density and no point mass. An extension of such a procedure, more relevant for turbulence phenomena, randomizes the allocation of mass between subintervals and another procedure, also of relevance for turbulence research, may also be employed with arbitrary distribution of multipliers (with mass being conserved either at each stage of the process or preserved only on the average) yielding multiplicative measures characteristic of multifractals. The relevance of such cascade processes in turbulence is discussed in, for example, [8, 16].

Multifractality of measures is easily extended to functions so that a stochastic process $X(t)$ is called multifractal if it has stationary increments and satisfies

$$E(|X(t)|^q) = c(q)t^{\tau(q)+1},$$

for all t and q belonging to intervals on the real line, and where $\tau(q)$ and $c(q)$ are functions with domain on the real line. The function $\tau(q)$ is called the scaling function of the multifractal process. It may be easily proved that $\tau(q)$ is concave, and for self-similar processes, controlled by one exponent H, it assumes a simple form

$$\tau(q) = Hq - 1,$$

with H known as the Hurst exponent. The corresponding process is called monofractal. For multifractal processes $\tau(q)$ is nonlinear. The Legendre transform of the scaling function $\tau(q)$ is called the Legendre multifractal spectrum:

$$f(\alpha) = \inf_q[\alpha q - \tau(q)].$$

In the above expression α is the local Hölder exponent, whose meaning may be defined in the following way. Let $\epsilon(t)$ denote the measure given either by expression (6) or expression (7) at

time $t \in [0, T]$ so that the infinitesimal variation of measure ϵ around time t is heuristically of the form

$$|\ln \epsilon(t + \mathrm{d}t) - \ln \epsilon(t)| \sim C_t(\mathrm{d}t)^{\alpha(t)},$$

where $\alpha(t)$ is called the local Hölder exponent, while C_t is the prefactor at t. From this definition it is apparent that $\alpha(t)$, also known as local scale at t, quantifies the scaling properties of the process at a given point in time so that lower values correspond to more abrupt variations. Multifractal processes contain a continuum of local scales and such a continuum is reflected in the smooth Legendre spectrum $f(\alpha)$. Hence the multifractal spectrum represents a convenient representation for the distribution of Hölder exponents. The shape of the spectrum is very sensitive to the distribution of multipliers so that it may give important information about multiplicative processes.

2.1. Large deviation spectrum

As mentioned earlier, the multifractal spectrum evaluated by performing the Legendre transform of the scaling function is a smooth function of local Hölder exponents. However sometimes more information may be obtained from the multifractal spectrum derived by applying the large deviation theory. Noticing that the Hölder exponent may be defined as the lim inf of the ratio

$$\ln |\epsilon(t + \Delta t) - \epsilon(t)| / \ln(\Delta t) \quad \text{as} \quad \Delta t \to 0,$$

it is suggestive to estimate the distribution of local Hölder exponents at a random instant. For that reason partition $[0, T]$ into 2^k subintervals $[t_i, t_i + \Delta t]$, where length $\Delta t = 2^{-k}T$, and calculate for each subinterval the *coarse Hölder exponent*

$$\alpha_k(t_i) \equiv \ln |\epsilon(t_i + \Delta t) - \epsilon(t_i)| / \ln(\Delta t),$$

so that a set $\{\alpha_k(t_i)\}$ of 2^k observations is formed. The range of Hölder exponents is then divided into small intervals $\Delta\alpha$, and let $N_k(\alpha)$ be the number of coarse exponents contained in $(\alpha, \alpha + \Delta\alpha]$. Proceeding further, one could calculate a histogram with relative frequencies $N_k(\alpha)/2^k$, which for $k \to \infty$ converge to the probability that a random time moment t has Hölder exponent α. However since multifractals typically have a dominant exponent α_0 implying that $\alpha(t) = \alpha_0$ at almost every instant, the obtained histogram would degenerate into a delta function, failing to give relevant information on a multifractal process. Instead, the multifractal spectrum in the context of the large deviation principle [15], denoted as large deviation spectrum (LDS), is defined as

$$f_{\mathrm{LDS}}(\alpha) := \lim_{k\to\infty} \sup \frac{\ln N_k(\alpha)}{\ln 2^k},$$

so that it represents the renormalized probability distribution of local Hölder exponents. Indeed, $N_k(\alpha)/2^k$ defines a probability distribution on $\{\alpha_i : i = 0, ..., 2^k - 1\}$. Referring to the law of large numbers and the arguments given earlier, it is expected that this distribution is concentrated more and more about the most expected value as k increases so that $f_{\mathrm{LDS}}(\alpha)$ measures how fast the probability $N_k(\alpha)/2^k$ to observe an atypical value of α decreases, i.e. $N_k(\alpha)/2^k \simeq 2^{f(\alpha)-1}$. As far as the LDS of multiplicative measures is concerned, it directly depends on the asymptotic distribution of α_k which in turn depends on the distribution of multipliers. Actually, most of the mass of the multiplicative cascade concentrates on intervals with Hölder exponents bounded away from the most probable value α_0, so that the LDS gives important information on these 'rare events'. A usually determined Legendre multifractal spectrum is concave by definition and represents the convex hull of the LDS.

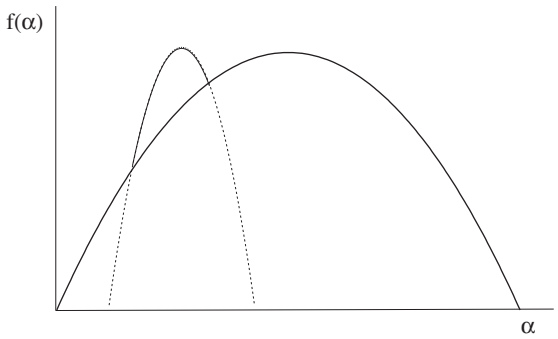

Figure 2. The spectrum of the lumping of two measures is the maximum of the individual spectra. The resulting spectrum shows clear signs of lumping and is not concave.

2.2. Atypical shapes of spectra

The most simple example for which the spectrum does not exhibit a smooth concave shape is the sum of two measures $\mu = \mu_1 + \mu_2$. If the supports of μ_1 and μ_2 are disjoint, the spectrum of their sum is the maximum of individual spectra with lumps corresponding to each measure and this mechanism of concavity deformation in the LDS is illustrated in figure 2 [17]. Naturally, a generalization to the superposition of more than two measures leads to more lumps and a more irregular (wavy-like) shape of the spectrum. The effects are similar to the ones observed in figures 5 and 6. In such a case the construction of two or more measures is identical from the geometrical point of view, however, the difference stems from the choice of multipliers. The nonconcave shape of the spectrum may also be explained in terms of a phase transition. Namely, at the α-value where the departure from concavity occurs, the major contributor to the set of singularities changes from one measure to the other.

In general, the departure from concavity of the LDS indicates diversity of multiplicative laws and evidence for the existence of several measures following such laws.

3. Large deviation spectra of plasma turbulence intermittency

The goal of this section is to present a comparative study of large deviation spectra of the boundary plasma turbulence intermittency in the SOL. The ion saturation current fluctuations of reciprocating Langmuir probe installed at the edge of magnetic confinement devices are used for this purpose. Recent experimental studies have suggested that intermittency in the SOL of magnetic confinement devices is caused by nonlocal coherent structures denoted as blobs

or avaloids [18], which essentially are large-scale structures with high radial velocity, ejected radially towards the wall and encountered intermittently in SOL. These structures lead to a direct loss of matter and energy and hence have a high impact on confinement in contrast to the second type of coherent structures which may exist in fusion devices, which represent locally organized fluctuations and which, due to their nonradial propagation, contribute less to the loss of confinement. We study intermittency properties of two different devices, the MAST spherical tokamak (L- and dithering H-mode) and the Tore Supra tokamak with limiter configuration (L-mode).

Spectra presented here were generated by consistent use of the measure given by (6) although both measures given by expressions (6) and (7) yield identical large deviation spectra so they may be used interchangeably.

3.1. MAST spectra

The datasets analysed here consist of measurements of the ion saturation current (I_{SAT}) performed by the moveable Langmuir probe located at the outboard midplane on the MAST device [19, 20]. The sampling rate was 1 MHz and during the discharge the distance from the plasma edge to the probe changed slowly. For this reason, time periods during which the distance was approximately constant so that plasma current and confinement modes were constant were chosen for the analysis. The analysis of two confinement regimes, L-mode and dithering H-mode, is presented here. Discharge 6861 is high density L-mode plasma and 9031 represents a dithering H-mode with heating power close to the threshold for L–H transition with intermittent high frequency edge localized modes (ELMs). Time-series of L-mode and dithering H-mode signals are presented in figures 3 and 4, respectively. Other relevant discharge parameters are presented in table 1.

The large deviation spectra for the 6861 L-mode and the 9031 dithering H-mode are presented in figures 5(*a*) and (*b*), respectively, on five different scales, namely, for $\Delta t = 2^3, ..., 2^7$. Measures given by expressions (6) and (7) yield identical spectra. In figure 6 these two spectra, for $\Delta t = 2^3, 2^4, 2^5$, are presented together for easier comparison. The most striking feature of these spectra is their departure from a pure bell-shape and concavity and is a good example where large deviation spectra provide more information than Legendre spectra, which are strictly concave although they may be asymmetrical. Their shape reflects the existence of several multiplicative laws underlying the cascade processes so that there is a lumping of measures whose supports are disjoint. It is evident that the L-mode has more complex multifractal structure in the sense that there are more α-values at which the irregularity of the spectrum occurs (i.e. more phase changes) than in the case of dithering H-mode. Hence, more measures are lumped and consequently the cascade mechanism and energy transfer is more complex in the case of the L-mode. The right-hand slope of the spectra, both in the case of the L- and the L/H- mode, is larger than the left-hand slope, indicating a rich variety of strong singularities and their gradual probability of occurrence.

When α is less than the most probable value of Hölder exponent α_0, it corresponds to divergent singularities since $\epsilon(t) \to \infty$ as $t \to 0$, while when $\alpha > \alpha_0$ it reflects regular

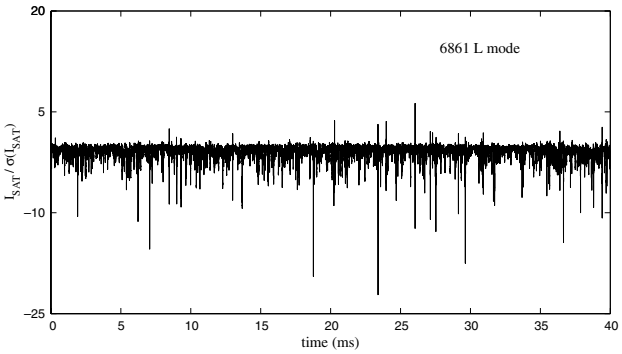

Figure 3. Normalized ion saturation current fluctuations as a function of time for the low confinement regime 6861 of the MAST device.

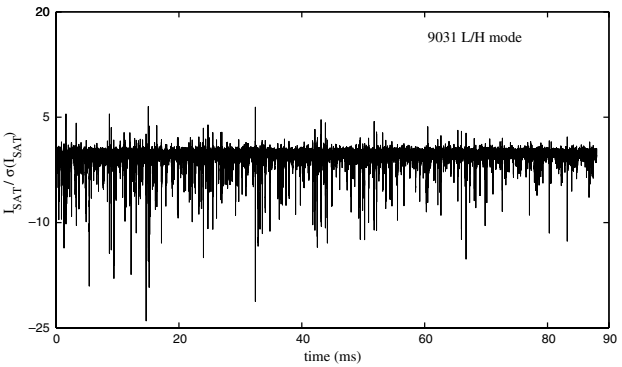

Figure 4. Normalized ion saturation current fluctuations as a function of time for the dithering H mode confinement regime of the MAST device.

(bounded) singularities since $\epsilon(t) \to 0$ as $t \to 0$. The fact that both spectra are not symmetric again emphasizes the fact that the processes involved are not purely multiplicative. This implies that the energy across scales is not transported through the generation of vortices and hence that it is not conserved at each step of the process, although it may be conserved on the average. This is closely related to random multiplicative cascades mentioned earlier with mass being conserved not at each stage of the process but on the average. The width of the spectrum, defined as the $|\alpha_{max} - \alpha_{min}|$, is larger in the case of the L-mode, due to the stronger intermittency effects. Moreover, more irregular instants (degenerate singularities) of fluctuations are present in the L-mode than in the dithering H-mode since in the former case the width $|\alpha_{min} - \alpha_0|$ is larger than in the latter case. Note also the location of the most probable Hölder exponent α_0, as $\alpha_0 \sim 0.6$ for the L-mode and slightly larger $\alpha_0 \sim 0.7$ for the dithering H-mode. As mentioned earlier, the shape of the spectra is determined by the distribution of multipliers of the multiplicative process and this issue will be addressed in detail elsewhere [21].

As a final remark we mention that measures in expressions (6) and (7) proposed here as multifractal dissipation measures for different dyadic intervals $\Delta t = 2^k (k = 1, 2, ...)$ produce large deviation spectra whose most probable Hölder exponents coincide, which is not the case for other measures, such as (4) or (5). Hence, evaluation of large deviation spectra, in addition to two-point correlation functions, supports the choice

Table 1. Discharge parameters for MAST data.

	Plasma current (kA)	Normalized electron density n_e/n_G	Probe distance from plasma edge (cm)	Duration of signal (ms)
6861 L	665	0.69	4.4 ± 0.1	40
9031 L/H	535	0.42	5.7 ± 1.0	88

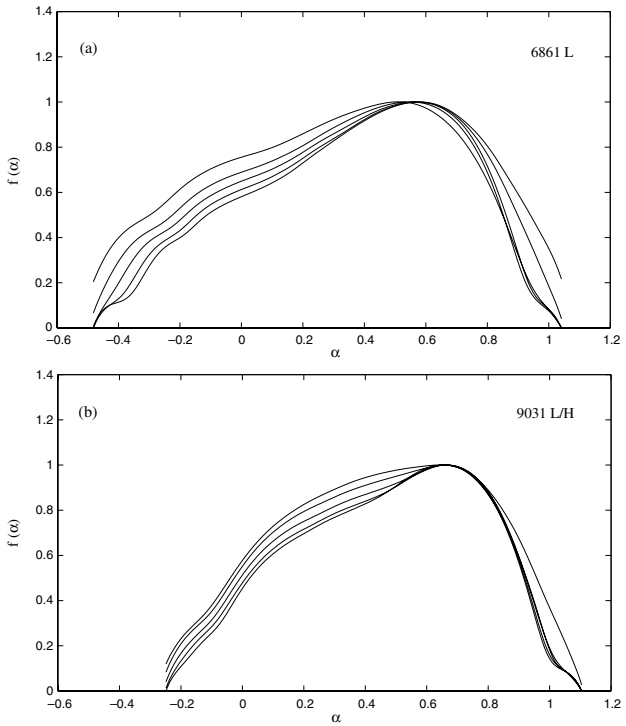

Figure 5. (*a*) LDS of the L-mode signal 6861 of the MAST device for five different scales $\Delta t = 2^3, ..., 2^7$. Lumping of measures is evident for singularities smaller than the most probable Hölder exponent. (*b*) LDS for the dithering H-mode signal 9031 of the MAST device for $\Delta t = 2^3, ..., 2^7$. Measures given by expressions (6) and (7) yield the same spectra. On both diagrams LDS curves corresponding to different Δt values may be identified at the left end of the spectra. The innermost spectrum corresponds to $\Delta t = 2^3$ while the outermost corresponds to $\Delta t = 2^7$ with the spectra in between corresponding to progressively increasing Δt values.

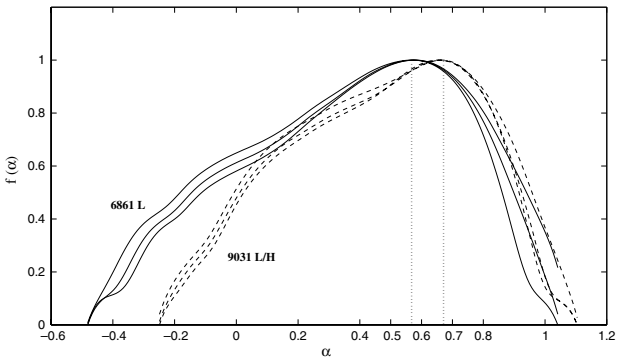

Figure 6. Direct comparison of large deviation spectra presented in figures 5(*a*) and (*b*) for $\Delta t = 2^3, 2^4, 2^5$. At the left end the innermost spectrum corresponds to $\Delta t = 2^3$ while the outermost corresponds to $\Delta t = 2^7$.

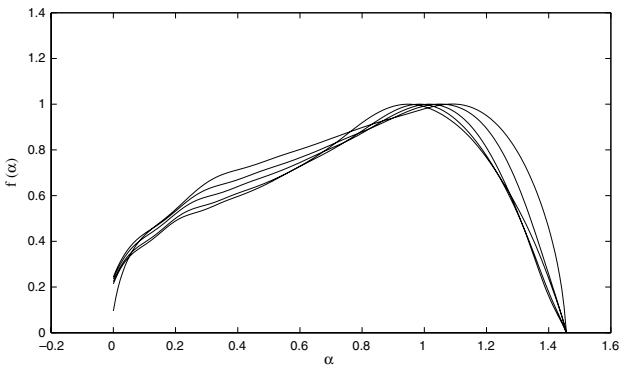

Figure 7. LDS for $\Delta t = 2^3, ..., 2^7$ of the L-mode 6861 obtained from measure (4). The position of the most probable Hölder exponent α_0 is shifted for each dyadic interval Δt. The same spectra are obtained from measure (5). Due to this shifting effect the measures (4) and (5) are not suitable for evaluation of LDS. As in figures 5 and 6, at the left end the innermost spectrum corresponds to $\Delta t = 2^3$ while the outermost corresponds to $\Delta t = 2^7$.

for these measures. An illustration of the LDS obtained by the application of the measure given by expression (4) is shown in figure 7. Note that the position of the most probable Hölder exponent α_0 is shifted for each dyadic interval Δt. This same undesirable effect is seen in the LDS obtained from measure (5).

3.1.1. Tore Supra spectra. The data were collected on the Tore Supra tokamak, a fusion device with a major and minor radii equal to $R = 2.32$ m and $a = 0.76$ m, respectively. The reciprocating Langmuir probe, installed on the top of the Tore Supra tokamak, contains two sets of three composite carbon tips with 6 mm diameter toroidally separated by a distance of 20 mm. The probe is immersed into the plasma of SOL at a predetermined position and comes back in $\sim$ 150 ms. Several plunges are performed during each discharge and 8000 data points were recorded at a frequency of 1 MHz. A detailed description of probes and data acquisition procedure is provided in [14]. Four different signals, each of 8 ms duration, are analyzed here and are shown in figure 8.

In the evaluation of large deviation spectra both measures (6) and (7) were used and compared. Again, no difference was noticed. Large deviation spectra of the four signals are presented in figures 9(*a*)–(*d*). As in the case of MAST turbulence data, rather than looking at the exact values of the LDS spectra a considerable amount of information may be obtained by inspecting the shape of the spectra. The most striking feature in the spectra is nonexistence or very mild lumping of measures with no superposition of measures. This is in great contrast to the MAST intermittency where lumping of measures is the most noticeable feature in the shape of the spectra. More interestingly, the mild lumping

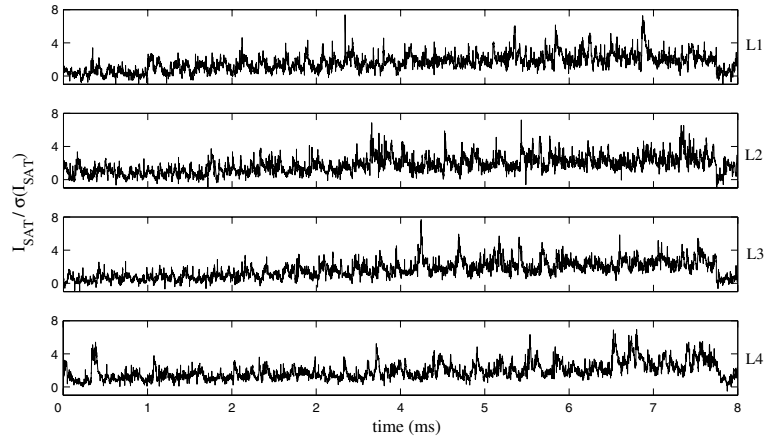

Figure 8. Normalized saturation current fluctuations as a function of time for the low confinement regime in the Tore Supra device. Data L1, L2, L3 and L4 were taken during plunges 1, 2, 3 and 4, respectively.

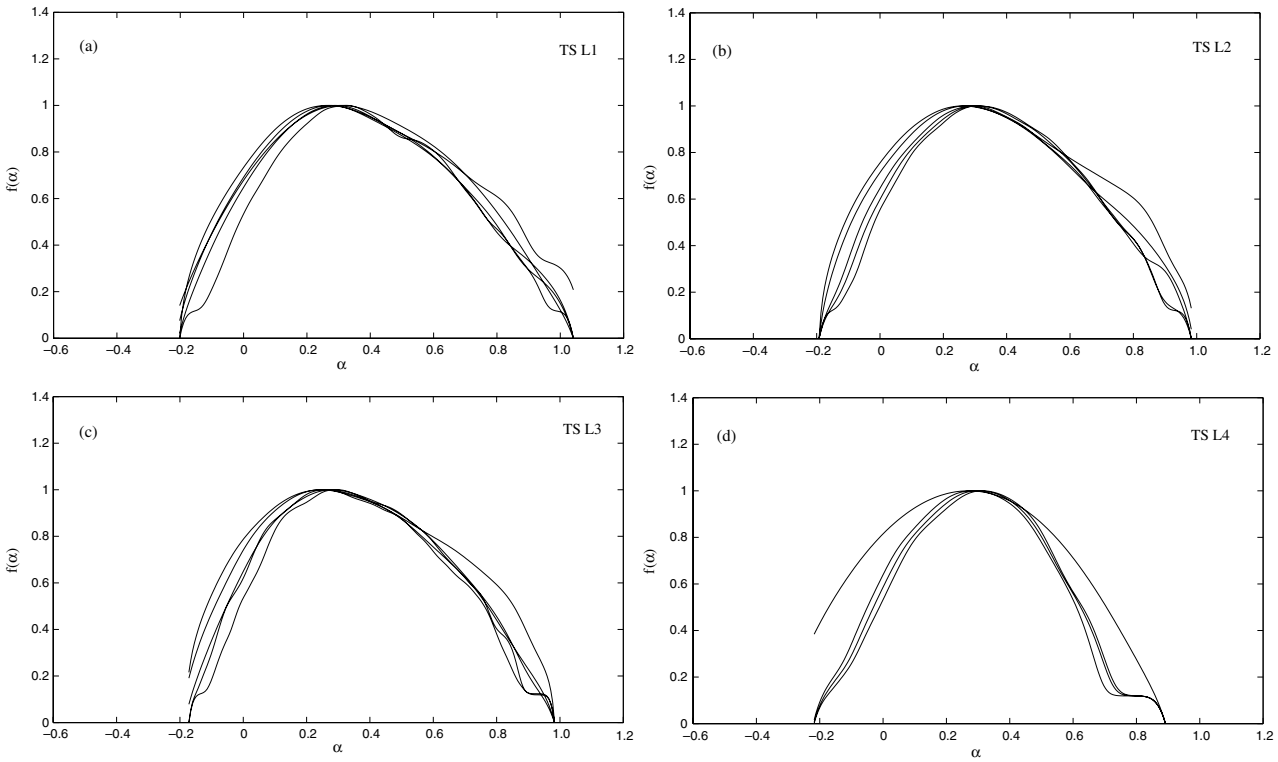

Figure 9. Large deviation spectra for the L-mode signals (*a*) L1, (*b*) L2, (*c*) L3 and (*d*) L4 of the Tore Supra device. The spectra are almost symmetric with respect to the most probable singularity value and practically there is no lumping of measures. The obtained spectra are the same when either of the two measures (6) or (7) is used. In all diagrams the innermost spectrum corresponds to $\Delta t = 2^3$ while the outermost corresponds to $\Delta t = 2^7$ with the spectra in between corresponding to progressively increasing Δt values.

occurs for measures corresponding to regular singularities while strong lumping in MAST intermittency corresponds to divergent singularities. The overall shape of the spectra and the arguments given above lead to the conclusion that statistical distribution of multiplicative cascade multipliers is completely different in the case of Tore Supra edge turbulence as compared with the MAST case implying different energy transport processes and different nonmultiplicative mechanisms which accompany energy transfer across scales in two devices. Without getting into details of calculations, we mention here that distribution of multipliers of the multiplicative cascade in the MAST turbulence is exponential while for the Tore Supra device it is log-normal [21]. Another important feature of the Tore Supra spectra is their smaller width $\alpha_{\max} - \alpha_{\min}$. However, more striking is the smaller range of divergent singularities $|\alpha_{\min} - \alpha_0|$, corresponding to the smaller number of rare fluctuations. Hence, not only is the edge intermittency weaker in Tore Supra fluctuations, it is less abundant in rare events.

Based on the above comparative analysis, in spite of the universal multifractal character of fluctuations, there are significant differences with important implications and care must be taken when generalizing certain properties of

fluctuations and when turning to specific features characteristic of a distinct device. Proceeding further with the aim of better understanding edge turbulence properties in fusion devices we undertake the analysis, presented in the next two sections, to provide time localized information about the essential frequency content of the fluctuations and about the existence of inertial range.

4. Estimation of local turbulence properties

Turbulent fluctuations, although highly nonstationary, usually exhibit approximate stationarity in the appropriately chosen segments within which spectral densities exhibit approximate power law scaling. Estimation of the power law behaviour of spectral densities from measured plasma edge fluctuations is based upon appropriate segmentation of the data and the choice of frequencies over which the search for power law behaviour is performed. The analysis presented here is based on the method and software presented in [22]. The motivation for such a procedure is twofold. The first is to estimate the local temporal variations in the correlation properties of the fluctuations and to evaluate the variation of the absolute level of these correlations. The second is the propagation of microwaves in plasma for the purpose of Doppler reflectometry used for estimating plasma rotation profiles and turbulence properties. Turbulent plasma medium essentially possesses multifractional properties as described in the previous sections, for example. However, it may be modelled locally in time or space, by self-similar (monofractal) fBm within the appropriately chosen temporal (or spatial) segments. Since the temporal (spatial) aspect matches the type of data which is analyzed, only the temporal viewpoint is applied here.

FBm represents the most simple local power law process which is nonstationary with stationary increments. The variance of the stationary increments is quantified by the structure function given by

$$E\left\{(B_H(t+\Delta t)-B_H(t))^2\right\}=\sigma^2|\Delta t|^{2H}, \qquad H\in[0,1]. \tag{8}$$

In the above expression the Hurst exponent H determines the correlation distance for the increments of the process and the quantity σ^2 quantifies the absolute level of correlations. Ordinary Brownian motion is characterized by a unique exponent $H=1/2$, so that regarding its multifractal properties $B_H(t)$ has a local Hölder exponent $\alpha(t)=H$, i.e. it is a monofractal process. FBm is self-similar since $B_H(t)=a^H B_H(t/a)$, where the equal to sign implies equality in distribution. Increasing the exponent beyond this value, i.e. $H>1/2$, corresponds to positive correlations (persistence) and long memory, while the case of $H<1/2$ corresponds to negative correlations (antipersistence). On a set of Lebesgue measure 1, the multifractal process with $H>1/2$ is more regular than a Brownian motion.

A pseudo-spectrum may be associated with fBm by removing the low frequencies [22], [23]. Let

$$X=B_H*\psi,$$

where the star denotes convolution and ψ a function that integrates to zero so that its Fourier transform Ψ vanishes at zero frequency. Although B_H is nonstationary, the process X is stationary and its power spectrum is

$$P_X\propto\sigma^2|\omega|^{-(2H+1)}|\Psi(\omega)|^2.$$

Power law processes are usually observed through a filter that cuts off very low frequencies so a power law may be associated with fBm

$$P_{B_H}\propto\sigma^2|\omega|^{-(2H+1)}. \tag{9}$$

In the Kolmogorov case $H=1/3$ the spectrum is

$$P_{B_H}\propto\sigma^2|\omega|^{-5/3},$$

over some range of frequencies denoted as inertial range.

Since fBm is a self-similar process, expression (8) yields unique parameter values for H and σ which characterize the process in its entirety so these parameters may be described as global. Since we are dealing with intermittent phenomena which exhibit multifractal properties equation (8) may be used to model plasma turbulence only in the restricted temporal domain in which turbulent signal is self-similar. Evaluation of parameters σ and H using equation (8) would therefore be hindered by the requirement to detect temporal domains in which this expression is valid. A more functional approach is to detect a range of frequencies over which the power law (9) pertains and then evaluate the parameters from the same expression. Wavelet scale spectra are used for this purpose because they provide time-scale decomposition that is compliant with power law processes, independent of their stationarity. Moreover, they are more flexible and adjustable to self-similar processes as verified in numerous studies, e.g. [24]. Parameters of the power law model, σ and H, are functions of time and these variations are modelled as a secondary stochastic process in our approach. Naturally, the model is applied only over a subset of scales known as the inertial range. Usually multifractal data, besides variations in σ and H, show variations in the inertial range itself. As explained in the introduction, turbulence in plasma is created and damped at the same spatial location so the existence and extent of the inertial range need conclusive tests which we set as one of the goals of this study.

The main steps in estimation of local turbulence properties are the following.

1. Partitioning of data into segments of equal temporal extent within which turbulent signal is approximately stationary. A special filtering procedure is devised in order to remove dependence of the estimated parameters on segmentation.
2. Wavelet decomposition of the data and evaluation of the scale spectra within each segment.
3. Determination of the inertial range of the scale spectra and evaluation of the power law parameters based on the fBm model. The turbulent data corresponding to the inertial range are assumed to be statistically well represented by fractal Brownian motion. Local turbulence parameters σ and H are therefore determined from the scale spectra corresponding to the inertial range. The extent of the inertial range varies from segment to segment and is rarely equal to the segment size. Since inertial range exists over specific scales (or equivalently over the corresponding time range) evaluated parameters have local character.

Important issues, relevant for interpretation of results, such as the choice of segmentation and filtering to smooth out the effects of segmentation, are described in detail in [22] and [25]. The intervals of stationarity are determined from a variogram (second order structure function) analysis of the wavelet coefficients. We have checked the filtering procedure to remove the effects of segmentation by choosing partitions which are short relative to the estimates of stationarity as well as the ones comparable to the intervals of stationarity. The results obtained were independent of segmentation so that no variability of the estimated parameters was detected.

4.1. Scale spectrum

Haar wavelets with narrow support, defined by

$$\psi(t) = \begin{cases} -1 & \text{if} \quad -1 \leqslant x \leqslant -1/2, \\ 1 & \text{if} \quad -1/2 \leqslant x < 0, \\ 0 & \text{otherwise}, \end{cases}$$

are a good choice for the analysis of turbulence due to their simplicity and versatility, however other bases would also be suitable. Let

$$n = (a_0(1),\ a_0(2),\ ...,\ a_0(2^M)$$

denote the plasma density data, i.e. ion saturation current where a_0 are level zero approximation coefficients

$$a_0(i) = \int_{i-1}^{i} n(t)\,\mathrm{d}t.$$

Detail wavelet coefficients corresponding to the signal are then calculated and the scale spectrum of n, relative to the Haar wavelet basis, is the sequence S_j defined by

$$S_j = \frac{1}{2^{M-j}} \sum\nolimits_{i=1}^{2^{M-j}} (d_j(i))^2, \qquad j = 1, 2, ..., M,$$

where j denotes the scale and d_j are detail coefficients given by

$$d_j(i) = \frac{1}{\sqrt{2^j}} \int_{-\infty}^{\infty} \psi(t/2^j - i) n(t)\,\mathrm{d}t.$$

The scale spectral point S_j is the mean square of the detail coefficients at scale j so that the spectrum can be interpreted as representing energy of the signal at different scales. If the inertial range exists the scale spectrum will exhibit linear scaling over a certain scale range $j_1 \leqslant j \leqslant j_2$. The main goal now is to test whether this inertial range can be modelled in a statistically satisfactory manner by a power law model with well-known properties. For the fBm process the scale spectrum, denoted as $S_j^{B_H}$, is linear in the log–log plot, assuming that the record is long enough. Actually, over a suitable range of scales the mean of the log scale spectrum is given by expression

$$E(\log(S_j^{B_H})) \approx c - p \log K_j,$$

where $p = -(2H + 1)$, $c = c(H, \sigma)$ is a known function and K_j is a temporal frequency

$$K_j = \frac{1}{\tau_j},$$

with $\tau_1 = 1\,\mu$s (the lowest temporal resolution of the data analyzed here). Hence, local Hurst exponents may be calculated readily from the slope of the log scale spectrum. Of particular interest is the value of $H = 1/3$ which corresponds to Kolmogorov's scaling.

Summarizing, the fBm scaling properties are used for determination of a local power law process. For processes under study, the power law (the exponent or slope) and the multiplicative constant (log intercept of the scale spectrum) are not constants. Instead, they both vary from segment to segment as would be expected in a multifractal signal. The procedure requires estimation of the inertial range whose existence and extent also change with time. Turbulence parameters, Hurst exponent H and parameter σ are calculated for each temporal segment over scales for which the inertial range exists.

4.2. Statistics of the scale spectrum

Statistics of the Haar wavelet coefficients for fBm and the power law estimates based on these statistics are presented based on the detailed exposition given in [22]. We assume that the data (ion saturation current in this case) corresponding to the inertial range are the set of wavelet approximation coefficients at level zero, that is

$$a_0(i) = \int_{i-1}^{i} B_H(t)\,\mathrm{d}t,$$

where B_H is fBm $\{B_H(t);\, t \geqslant 0\}$. The wavelet coefficients are normally distributed random variables with

$$E[d_j(i)] = 0, \tag{10}$$

$$\mathrm{Var}[d_j(i)] = \sigma^2 \frac{(1 - 2^{-2H})}{(2H + 2)(2H + 1)} 2^{j(2H+1)},$$

$$\mathrm{Corr}[d_{j_1}(i_1) d_{j_2}(i_2)] = \frac{|D/\sqrt{l}|^{2H+2}}{8(2^{2H} - 1)} \left\{\delta_{l/D}^2 \delta_{1/D}^2\, |t|^{2H+2}\right\} |_{t=1}.$$

Here

$$l = 2^{j_2 - j_1}, \qquad j_1 \leqslant j_2,$$

is the relative scale,

$$D = |(2i_2 - 1)l - (2i_1 - 1)|,$$

is the relative location and

$$\delta_d^2 f(t) = f(t + d) - 2f(t) + f(t - d),$$

is the second order symmetric difference. Based on these properties of wavelet coefficients the mean of the scale spectra may be obtained

$$E[S_j] = E[d_j(i)^2] = \sigma^2 h(H) 2^{j(2H+1)},$$

where

$$h(H) = \frac{(1 - 2^{-2H})}{(2H + 2)(2H + 1)}.$$

Statistical properties of the logarithm of the scale spectra are necessary for the least squares fit of the power law and we summarize here only the most important results. In the large N_j limit ($N_j = 2^{M-j}$ the number of detail coefficients at level

j and 2^M the total length of the data), distribution of scale spectral points is normal

$$S_j^{B_H} = E[S_j^{B_H}]\left(1 + \frac{v_j}{\sqrt{N_j}}\right), \qquad (11)$$
$$v_j \sim \mathcal{N}(0, g(H)), \qquad \text{for } N_j \to \infty.$$

In the above expression $\mathcal{N}(\mu, s^2)$ is the normal distribution with mean μ and variance s^2,

$$g(H) = \lim_{N_j \to \infty}\left\{\frac{4}{N_j}\sum_{k=0}^{N_j-1}(N_j - k)\rho_H^2(k) - 2\right\},$$

and $\rho_H(k)$ is the correlation coefficient of wavelet coefficients at level k. Expression (11) leads to the asymptotic estimate

$$\log_2(S_j^{B_H}) = \log_2(E[S_j^{B_H}]) + \frac{v_j}{\sqrt{N_j}\ln(2)},$$

which may be written as

$$\log_2(S_j) = \log_2(\sigma^2 h(H)) + j(2H+1) + \frac{v_j}{\sqrt{N_j}\ln(2)}$$
$$= c + jp + \frac{v_j}{\sqrt{N_j}\ln(2)}, \qquad (j_1 \leqslant j \leqslant j_2).$$

The slope p and log intercept c are estimated from the data, while the fluctuation term $v_j/\sqrt{N_j}$ is given by the central limit theorem for the scale spectra for large N_j. Finally, the least square method yields estimates for the Hurst exponent H and parameter σ^2 as

$$\hat{H} = (\hat{p} - 1)/2,$$
$$\log_2(\sigma^2) = \hat{c} - \log_2(h(\hat{H})).$$

4.3. Local features of MAST and Tore Supra edge turbulence

For the MAST data the sizes of segments ranged from 256 μs to $\sim$ 2 ms, while for the Tore Supra partitioning was in the range 256 μs to $\sim$ 1 ms. The lower limit of the segment size is governed by the maximum temporal extent of the inertial range. No effects of partitioning on estimation of the inertial range or the turbulence parameters σ and H were detected due to the procedure for removal of segmentation dependent effects [22, 25].

Local turbulence modelling using fBm and wavelet basis scaling properties show that indeed inertial range in temporal domain exists and that it is possible to gain important information about edge turbulence properties using this approach. In particular, the scale spectra of MAST data reveal a similar distribution of scaling range values between 0.0078 and 0.0625 rad μs^{-1} (the corresponding temporal range is 32–256 μs) for both the L-mode and the dithering H-mode confinement. It would be reasonable to anticipate different distributions of inertial range values across segments for the case of L- and H-modes if not the minimal and maximal inertial range values (i.e. interval) themselves. In the dithering H-mode case, apparently the variability of the inertial range extent is enhanced by the switching process from low to high confinement, so that the distribution of inertial range values is practically the same as in the L-mode case. In figure 10 the inertial range of four segments for the case of L-mode 6861of

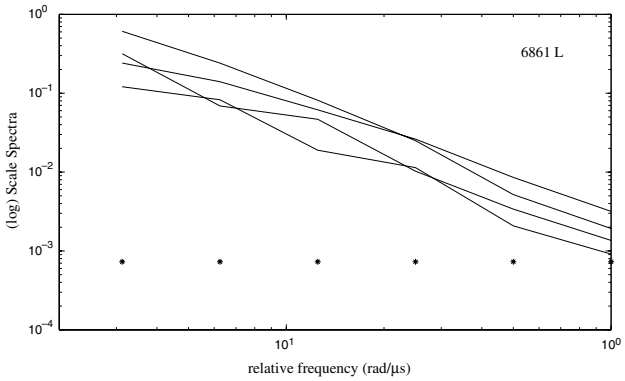

Figure 10. Scale spectra of several nonoverlapping approximately stationary segments of the L-mode signal 6861 in the MAST device. Stars represent reference Haar wavelet scales over which the power law applies, i.e. the extent of inertial range. The segment size is 512 μs while the scale spectra from top to bottom correspond to segments whose extent is 2048–2560 μs, 6144–6656 μs, 12800–13312 μs and 22016–22528 μs, respectively.

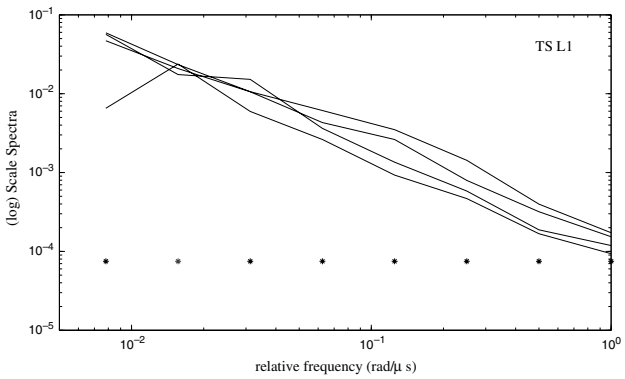

Figure 11. Scale spectra of approximately stationary nonoverlapping segments of the L-mode signal L1 in the Tore Supra device. Stars at the bottom represent reference wavelet scales over which the power law applies, i.e. the extent of inertial range. As in figure 10 the segment size is 512 μs while the scale spectra from top to bottom correspond to segments whose extent is 1536–2048 μs, 4096–4608 μs, 5632–6144 μs and 6656–7168 μs, respectively.

the MAST device is presented. In this and the subsequent figure, temporal frequency is

$$K_j = \frac{1}{\tau_j} = 2^{1-j},$$

while stars in the lower part of the graphs indicate the dyadic extent (the range of j-values) of the estimated inertial range. The corresponding temporal extent of the inertial range for the four segments presented is $\sim$ 32 μs. The minimum and the maximum scaling range values in the temporal domain for the Tore Supra data are the same as in the MAST data case, i.e. 32 and 256 μs. However taking all segments into account there are more inertial ranges of extent larger than or equal to 64 μs as compared with the MAST case. This is expected based on the more regular and more symmetric large deviation spectra, implying less strong intermittency in the Tore Supra edge turbulence data. In figure 11 the inertial range of four segments of the L-mode (L1 signal) of the Tore Supra device is presented.

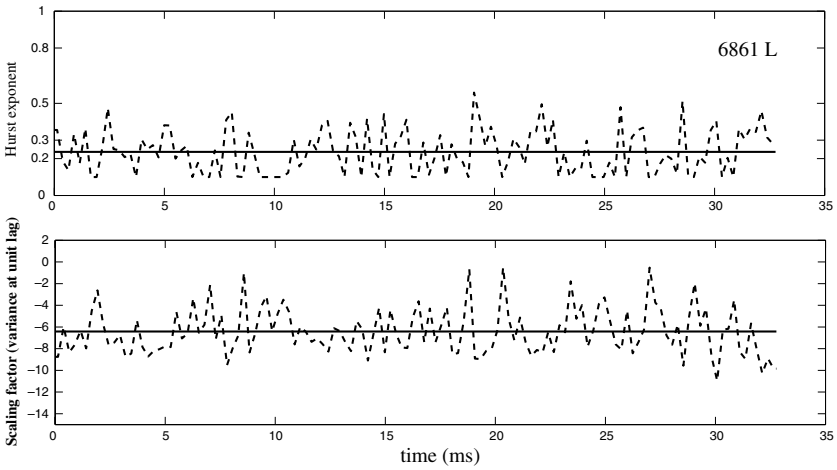

Figure 12. Parameters of the fBm model, Hurst exponent and the variance at unit lag, for the L-mode of MAST. Note random variations of each parameter reflecting multifractal character of the plasma density fluctuations. The smoothed values are represented by solid lines. Note that the Hurst exponent fluctuates around the smoothed value $H = 0.23$.

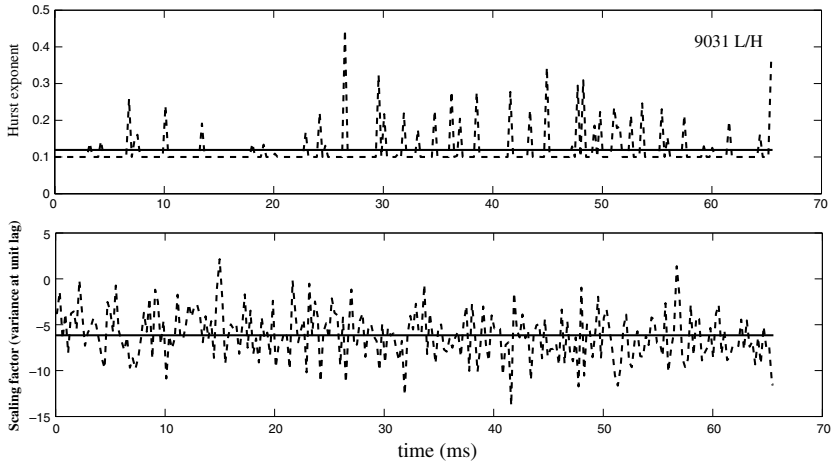

Figure 13. Parameters of the fBm model, Hurst exponent and the variance at unit lag for the dithering H-mode in MAST. Note random variations of each parameter reflecting multifractal character of the plasma density fluctuations. The smoothed values are represented by solid lines. Note the considerably lower value of the Hurst exponent than in the case of the L-mode.

Based on the fBm wavelet model (11), temporal variations of the local Hurst exponent and the variance for the case of L- and dithering H-mode MAST are presented in figures 12 and 13, respectively. Both parameters show random fluctuations with local Hurst exponent fluctuations closer to Kolmogorov's value of 1/3 in the L-mode than in the H-mode case, so that from that aspect of multifractality L-mode turbulence is similar to the neutral fluid turbulence. In the case of the dithering H-mode, figure 13, the average Hurst exponent value is lower than in the L-mode case, however, it exhibits distinct random variability from a minimum value of $H = 0.1$. Both cases are typical of multifractal processes which show fast, random fluctuations of the regularity parameter H.

Characteristics of local turbulence of the Tore Supra device are presented in figures 14 and 15, where cases (plunges) L1 and L4 are illustrated. Data L2 and L3 are not presented since they are very similar to the L1 case. The striking feature on both diagrams is the slow, almost deterministic variation of the local Hurst exponent and the variance. For L4 data, variability is somewhat larger, but it is almost periodic so that it reflects the deterministic like character of the L1 case. We may conclude that local processes in figures 14 and 15 display enough regularity which are not characteristic of the true multifractals. Actually, these sets of Tore Supra edge turbulence data are *multifractional*, rather then multifractal. This is the term used for processes which are not multifractal in the true sense since they may exhibit local irregularity as reflected in the H value that is 'deterministic', meaning that it is almost the same or predictable for all realizations, whereas it is random for truly stochastic processes. Moreover, H varies smoothly or very slowly while this is not the case in a true multifractal process. Some of these features may have been anticipated based on the shape of large deviation spectra, however, analysis local in time or in space provides, besides additional information, necessary conclusiveness.

5. Conclusion

Multifractal tools have been employed in order to test the universality of the edge turbulence properties in various magnetic confinement devices. It was shown that large

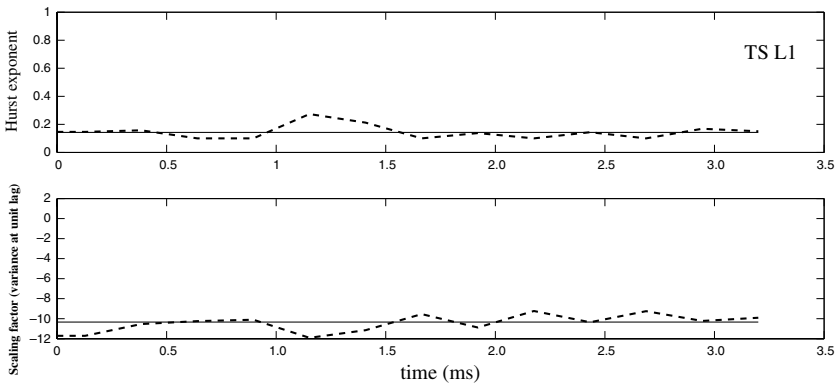

Figure 14. Parameters of the fBm model, Hurst exponent and the variance at unit lag, for the L1 fluctuations of the Tore Supra device. Note smoother, almost deterministic variations of each parameter in comparison with random fluctuations in the MAST case.

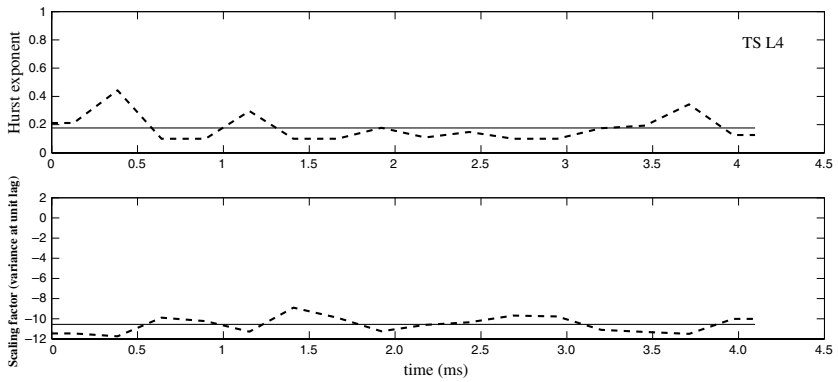

Figure 15. Parameters of the fBm model, Hurst exponent and the variance at unit lag, for the L4 signal of the Tore Supra device. Variations of these parameters is the largest among the Tore Supra data, although almost periodic variations in both parameters are readily noticeable.

deviation spectra represent powerful tools enabling advanced insight into the multifractal processes and provide information that is sensitive to the data and hence to the confinement device in which the data were generated. Complemented by an analysis of local turbulence based on the fBm and wavelet scaling properties it was shown that turbulence properties are different in the MAST device and the Tore Supra tokamak, suggesting that new studies involving different devices and possibly extensions of existing methods for the analysis should be undertaken. The shapes of large deviation spectra clearly suggest different energy transport mechanisms in the two devices while local analysis reveals a multifractional character of the processes in the Tore Supra device in contrast to the genuine multifractal processes in the MAST device. In the light of results presented here the call for a careful interpretation of the universal characteristics of edge turbulence data is evident. In addition, differences over local temporal records of turbulence data for various devices show how important local modelling based on the fBm and wavelet scale spectra is for constructing an accurate synthetic random medium for simulation of wave propagation in turbulent plasma.

Acknowledgments

One of the authors, M.R., expresses gratitude to the National Institute for Fusion Studies for hospitality and support under the NINS–NIFS International Base Research Network funding. Authors M.R. and M.S. also acknowledge partial funding by the Serbian Ministry of Science under grants OI 144022 and OI 141034, respectively. We thank Richard Dendy and Ben Dudson for providing the MAST data.

References

[1] Antar G., Counsell G., Yu Y., Lombard B. and Devynck P. 2003 *Phys. Plasmas* **10** 419–28
[2] Wang G., Antar G. and Devynck P. 2000 *Phys. Plasmas* **7** 1181
[3] Carreras B.A. *et al* 1998 *Phys. Plasmas* **5** 3632
[4] Budaev V.P., Takamura S., Ohno N. and Masuzaki S. 2006 *Nucl. Fusion* **46** S181–91
[5] Carbone V., Regnoli G., Martines E. and Antoni V. 2000 *Phys. Plasmas* **7** 445
[6] Carreras B., Lynch V.E., Newman D.E., Balbin R., Bleuel J., Pedrosa M.A., Endler M., van Milligen B., Sánchez E. and Hidalgo C. 2000 *Phys. Plasmas* **7** 3278–87
[7] Cloquet C., Xu Y.H., Van Schoor M., Jachmich S., Vergote M. and the TEXTOR team 2006 *Proc. 33rd EPS Conf. on Plasma Physics (Rome, Italy)* vol 301 P-2.155
[8] Frisch U. 1995 *Turbulence, the Legacy of A. N. Kolmogorov* (Cambridge: Cambridge University Press)
[9] Cleve J., Greiner M. and Sreenivasan K.R. 2003 *Europhys. Lett.* **61** 756–61
[10] Monin A.S. and Yaglom A.M. 1971 *Statistical Fluid Mechanics* vol 2 (Cambridge, MA: MIT Press)
[11] Cleve J., Greiner M., Person B.R. and Sreenivasan K.R. 2004 *Phys. Rev.* E **69** 066316
[12] Channal O., Chabaud B., Castaing B. and Hébral B. 2000 *Eur. Phys. J.* B **17** 309

[13] Delour J., Muzy J.F. and Arneodo A. 2001 *Eur. Phys. J.* B **23** 2443-8
[14] Antar G.Y., Devynck P., Garbet X. and Luckhardt S.C. 2001 *Phys. Plasmas* **8** 1612
[15] Riedi R.H. 1995 *J. Math. Anal. Appl.* **189** 462–90
[16] Menevau C. and Sreenivasan K.R. 1991 *J. Fluid Mech.* **224** 429
[17] Riedi R.H. and Vehel J.L. 1997 *Technical Report* 3129 INRIA Rocquencourt, France (available at www.dsp.rice.edu.)
[18] Antar G.Y., Krasheninnikov S.I., Devynck P., Doerner R.P., Hollmann E.M., Boedo J.A., Luckhardt S.C. and Conn R.W. 2001 *Phys. Rev. Lett.* **87** 065001
[19] Counsell G.F. *et al* 2005 *Nucl. Fusion* **45** S157–67
[20] Dudson B.D., Dendy R.O., Kirk A., Meyer H. and Councel G. F. 2005 *Plasma Phys. Control Fusion* **47** 885–901
[21] Rajković M., Škorić M. and Dendy R. 2008 Characterization of intermittency in plasma edge turbulence *Plasma Phys. Control. Fusion* at press
[22] Sølna K. and Papanicolaou G. 2002 Wavelet based estimation of local Kolmogorov turbulence in *Theory and Applications of Long-range Dependence* ed P. Doukhan *et al* (Boston: Birkhäuser) pp 473–506
[23] Abry P., Gonçalves P. and Flandrin P. Wavelets, spectrum analysis and 1/f processes in *Wavelets and Statistics (Springer Lecture Notes in Statistics vol 103)* ed A. Antoniadis and G. Oppenheim (New York: Springer) pp 15–29
[24] Abry P., Flandrin P., Taqqu M.S. and Weitch D. 2000 Wavelets for the analysis, estimation and synthesis of the scaling data in *Self Similar Network Traffic and Performance Evaluation* ed K. Park and W. Willinger (New York: Wiley-Interscience) chapter 2
[25] Papanicolaou G., Washburn D. and Sølna K. 1998 *Proc. SPIE* **3381** 256